NASA TR R-162

NATIONAL AERONAUTICS AND SPACE ADMINISTRATION

TECHNICAL REPORT
R-162

A THEORY OF SPACE-PROBE ENTRY UNDER CONDITIONS OF HIGH MASS LOSS

By FREDERICK C. GRANT

1963

For sale by the Superintendent of Documents, U.S. Government Printing Office
Washington, D.C., 20402—Price 30 cents

TECHNICAL REPORT R-162

A THEORY OF SPACE-PROBE ENTRY UNDER CONDITIONS OF HIGH MASS LOSS

By FREDERICK C. GRANT

Langley Research Center
Langley Station, Hampton, Va.

TECHNICAL REPORT R–162

A THEORY OF SPACE-PROBE ENTRY UNDER CONDITIONS OF HIGH MASS LOSS

By Frederick C. Grant

SUMMARY

A theory of velocity limitation is developed on the basis of a simple analytical model of a returning space probe. The limiting velocity is the lowest atmospheric entry speed for which the heat-protection material of the probe is entirely consumed. The geometry treated is a family of slender blunted cones moving in the direction of the axis. The face of the cone is assumed to be continuously vaporized by the flow. The entry speed is presumed to be so high that a large fraction (or all) of the vehicle volume is consumed in the entry. The entry speed is also high enough for the dominant mode of heat transfer to the vehicle to be through radiation from the hot gas cap at the nose. In the regime of radiation dominance, a second-order nonlinear differential equation is found which describes the geometric and dynamic history during atmospheric entry. By means of solutions of the basic size-altitude equation the velocity limit is traced out.

With a limiting form of the heat-input function, explicit formulas for the limiting velocity of the family of truncated cones are developed. The limiting velocity is found to be independent of the size of the probe but dependent on the shape. Pointed cones yield the highest limiting velocities for the class of probes considered. However, flat-faced cylinders yield values nearly as high. The proportions of the cylinders do not affect the limiting velocity, and therefore long rods and thin wafers have the same values. Only the altitude of the high-mass-loss region shifts with the probe size or with the cylinder proportions.

INTRODUCTION

Analyses of atmospheric entry in the satellite and escape speed ranges have not emphasized mass losses since the mass fraction devoted to heat protection is typically quite small. The case of low-mass-loss probe entry in the meteoric speed range was outlined in reference 1. At sufficiently high speeds in the meteoric speed range, however, the mass loss cannot be ignored for reasonably sized vehicles.

The basic contrasts between meteor entry and probe entry lie in the sizes, materials, and shapes. Meteorites are composed of iron or stone, reach enormous sizes, and seem to have irregular, blunt shapes. Probes, on the other hand, cannot weigh more than a few thousands of pounds, and the materials and shapes can be chosen as desired. For successful probes a definite fraction of the mass, the scientific payload, must survive the entry. Of course, in a sense, a meteorite is intrinsically a scientific payload.

The anticipated speeds of probe entry are well beyond the capability of shock tubes. Shock tubes are unlikely to achieve speeds much higher than the present limit of about 40,000 feet per second. Information on entry at higher speeds can, at present, be directly obtained only by observation of meteors. Recourse must be made to judicious extrapolation and to analytical methods for investigation of space-probe entry.

The problem of natural-meteor mechanics has been successfully treated, in the main without detailed consideration of the heat-input function. (See ref. 2, for example.) Although shock-tube experiments and theoretical analyses have produced realistic heat-input functions for simple shapes and it is now possible to include realistic heat-input functions in problems of entry mechanics, the range of applicability of the results for high-mass-loss trajectories is not known.

A critical regime in space-probe return is found near the low meteoric-velocity limit, the existence of which was suggested in reference 3. According to the analysis of reference 3, meteorlike bodies in the ballistic-parameter range of interest for space probes ($\sim 10^2$ lb/sq ft) are completely consumed when entry velocities are higher than roughly 50,000 to 60,000 feet per second.

It is the purpose of this paper to develop the theory of velocity limitation for probelike bodies. This means that a choice of physically reasonable shapes must be made and the survival of a definite fraction of the initial mass must be provided.

SYMBOLS

A reference area for drag evaluation

A_q area through which heat is transferred to probe

$a=\left(\frac{D}{2L}\right)^2$

a_g acceleration due to gravity, presumed constant

$b=\frac{1}{1-\mu}\left[1-\mu(1-\lambda_{\infty-})^3\right]$

C_D drag coefficient

D base diameter of vehicle

$F(\lambda)=2\int_0^\lambda f(\lambda)d\lambda$

$f(\lambda)$ ballistic function, $\frac{a_g h_s'}{2\delta}$

G deceleration in units of a_g

$g(\lambda)$ differentiable function of λ

$g'(\lambda)=\frac{dg}{d\lambda}$

h altitude

h_s scale height (the altitude change for which the density changes by the factor e, the base of natural logarithms)

h_s' scale height measured along flight path

$K=\frac{h_s'}{w\Delta W}\left(\frac{\bar{q}}{q_{st}}\right)_r \beta \frac{D}{L}$

L length of cone which is truncated to form vehicle; original cylinder length

l instantaneous length of shrinking vehicle

m vehicle mass

m_p payload mass

m, n, r, s exponents in heating-rate formulas

Q total heat transferred to probe

q heating rate per unit area

R original radius of sphere

r instantaneous radius of shrinking sphere

S surface area

t time

U vehicle velocity

V vehicle volume

ΔW heat of sublimation of heat-protection material per unit weight

w weight density of heat-protection material

z parameter to which $f(\lambda)$ is proportional

α, β constants in heating-rate formulas

γ flight-path angle with respect to horizontal

δ ballistic parameter, $\frac{ma_g}{C_D A}$

η fraction of kinetic-energy flux that enters the probe

λ dimensionless length of conical or cylindrical probe, l/L; dimensionless radius of spherical probe, r/R

μ payload fraction, $m_p/m_{\infty-}$

ρ mass density of atmosphere

ω natural logarithm of ρ

Subscripts:

$\infty+$ $\omega=\infty$

$\infty-$ $\omega=-\infty$

c convective

l limiting

max maximum

r radiative

st stagnation point

Dot over a symbol denotes the time derivative.

Bar over a symbol denotes the average value.

ANALYSIS

DYNAMIC EQUATION

The velocities and air loads are so high for the cases to be considered that the acceleration due to gravity will be neglected. Neglect of gravity implies that the motion is linear. Another assumption is that the entry is at such a steep angle that the curved surfaces of constant atmospheric density may be regarded as parallel planes for the straight flight paths to be considered. The atmosphere is to be approximated by an isothermal

model at constant acceleration due to gravity. Such a model has an exponential variation of density with altitude which may be expressed as

$$\frac{d\rho}{\rho}=-\frac{dh}{h_s} \tag{1a}$$

The parameter h_s is called the scale height of the atmosphere and may be defined as the altitude change for which the density changes by the factor e, the base of natural logarithms. For the simplified atmospheric-entry model under discussion, a generalized scale height h_s' may be defined as the distance along the flight path in which the density changes by the factor e. The two parameters are related simply by

$$h_s'(\sin\gamma)=h_s \tag{1b}$$

where γ is the angle of the flight path with respect to the horizontal.

The substitution of the density for time as the independent variable will be made as a matter of convenience. By combining the relations (1a) and (1b) the relation between t and ρ is found as

$$d\rho=\frac{\rho U}{h_s'}\,dt \tag{1c}$$

The equation of motion, if the vaporized probe material is assumed to leave with zero velocity with respect to the probe, is

$$-m\dot{U}=\frac{1}{2}C_D A\rho U^2 \tag{1d}$$

Equation (1d) becomes, after substitution of equation (1c),

$$-\frac{dU}{d\rho}=\frac{a_g h_s'}{2\delta}U \tag{1e}$$

where $\delta=\dfrac{ma_g}{C_D A}$ is the so-called ballistic parameter. Depending on the geometry chosen, the coefficient of U in the right member of equation (1e) is an, as yet, unspecified function of the nondimensional size λ of the probe. This functional relationship will be denoted as

$$f(\lambda)=\frac{a_g h_s'}{2\delta} \tag{1f}$$

so that the equation of motion has the form

$$-\frac{dU}{d\rho}=f(\lambda)U \tag{1g}$$

HEATING EQUATION

The differential heat input to the probe material will have the form

$$dQ\propto w\Delta W A_q dx \tag{2a}$$

where dx is the depth of vaporization over an area A_q. The same differential heat input in terms of flow variables will be assumed to be expressible in the form

$$dQ\propto\rho^r U^s A_q g_1(\lambda)dt \tag{2b}$$

where $g_1(\lambda)$ is a function of the nondimensional probe size λ. The functional form of g_1 depends on the analytical model. Combination of relations (1c), (2a), and (2b) yields the form

$$-\frac{d\lambda}{d\rho}=\rho^{r-1}U^{s-1}g(\lambda) \tag{2c}$$

In the present analysis the shrinkage equation will always be a special case of equation (2c).

SIZE-ALTITUDE EQUATION

The analysis takes a compact form if equations (1g) and (2c) are combined. By differentiation of equation (2c) and substitution of equation (1g) the following second-order size-altitude equation is found, which is the basic equation of the present analysis:

$$\frac{d^2\lambda}{d\rho^2}+\left[(s-1)f(\lambda)-\frac{r-1}{\rho}\right]\frac{d\lambda}{d\rho}-\frac{g'(\lambda)}{g(\lambda)}\left(\frac{d\lambda}{d\rho}\right)^2=0 \tag{3a}$$

An advantage of equation (3a) is that it is independent of the velocity, which appears explicitly only when fixing boundary values of the slope by the condition

$$-\frac{d\lambda}{d\rho}=\rho^{r-1}U^{s-1}g(\lambda) \tag{3b}$$

It is, for some purposes, more convenient to write equations (3a) and (3b) in terms of the variable $\omega=\log_e\rho$ which is linearly related to the altitude in an isothermal atmosphere at constant a_g. This transformation yields

$$\frac{d^2\lambda}{d\omega^2}+[(s-1)e^{\omega}f(\lambda)-r]\frac{d\lambda}{d\omega}-\frac{g'(\lambda)}{g(\lambda)}\left(\frac{d\lambda}{d\omega}\right)^2=0 \tag{3c}$$

$$-\frac{d\lambda}{d\omega}=e^{r\omega}U^{s-1}g(\lambda) \tag{3d}$$

Examination of the basic equation (3c) indicates some general properties of the solutions which lead to scaling laws with various parameters for quantities of interest. For example, for parameters which appear as factors of $g(\lambda)$, but do not appear in $f(\lambda)$, variation of these factors with no change in the product produces no change in the integral curve. A more general transformation is the change of the integral curves under the variation of any parameter z which appears as a factor of $f(\lambda)$. If we imagine an element of arc of an integral curve of equation (3c) to be translated in ω by an amount σ so that

$$\omega' = \omega + \sigma \tag{3e}$$

the coefficient of the linear term in $\frac{d\lambda}{d\omega}$ of equation (3c) undergoes the change

$$ze^{\omega} \rightarrow z'e^{\omega'} = z'e^{\sigma}e^{\omega} \tag{3f}$$

where $z \rightarrow z'$ in the translation. If we require of z' that

$$z = z'e^{\sigma} \tag{3g}$$

then the $\frac{d^2\lambda}{d\omega^2}$ term of differential equation (3c) is unchanged for the translated element. Thus any integral curve, when translated, is a solution for a different value of z. The functional dependence of certain quantities of interest follows directly from this invariance of the integral curves under a translation σ plus an associated change of z. Written in a form different from equation (3g), the proper association is

$$\rho z = \text{Constant} \tag{3h}$$

The transformation described by equations (3g) or (3h) will be called a ρ-z shift.

The character of the integral curves of the size-altitude equation (3c) for physically interesting cases is indicated in figure 1. Two semi-infinite regions of nearly constant nondimensional size λ are separated by a region of rapid λ change, the high-mass-loss region. In this narrow region occurs the heating pulse, the acceleration pulse, and the size-change $\left(-\frac{d\lambda}{d\omega}\right)$ pulse which peaks at the inflection point. The acceleration peak follows the inflection point. The limiting velocity is defined in terms of the limiting size on the right,

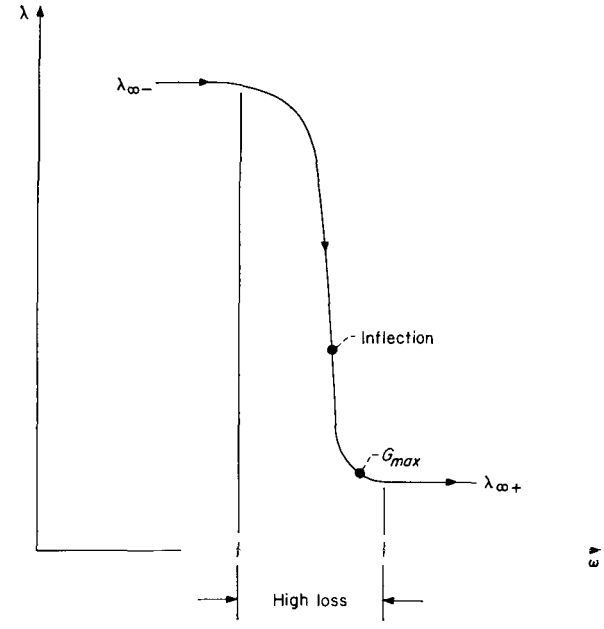

FIGURE 1.—Sketch of integral curve of size-altitude equation.

$\lambda_{\infty+}$. The velocity $U_{\infty-}$ (the value of U at $\omega = -\infty$) for which $\lambda_{\infty+}$ equals 0 is defined as the limiting velocity U_l. For higher velocity at $\omega = -\infty$ the vehicle will burn up at finite altitudes (unless the payload vanishes, which case, corresponding to meteorlike bodies, will be discussed subsequently).

Although the size-altitude equation can be regarded as a geometric relation, the terms have dynamic significance. The only term unequivocally favorable to probe survival is that with $f(\lambda)$ as coefficient, corresponding to loss of velocity and mass during entry. High values of $f(\lambda)$ are desirable, or alternatively, small values of $\delta_{\infty-}$ are desirable. More precisely, as will be seen later, it is a high mean value of δ^{-1} that is desirable.

ANALYTICAL MODEL

In view of the facts that high radiation intensities are associated with the large enthalpy changes in normal shock waves and that radiative heat transfer is increasingly dominant at space-probe (meteoric) speeds, it seems desirable that the surfaces of space probes should have small fractions of the surface area exposed to strong shock waves. This suggests that the basic shape of space probes, unlike that of meteors, should be slender so that strong shock waves can exist only at the foremost parts. A slender

blunted cone appears to be a possibility since the area of the blunted nose will increase with mass loss and the drag will thus increase at the lower velocities for which radiation intensity is lessened. Detailed analysis will show whether these simple considerations are justified.

Geometry.—The axisymmetric geometry is indicated in figure 2. The slope of the flanks of the cone with respect to the axis is so small that the heat absorbed by the flanks can be neglected in comparison with that entering the face. As the face recedes it is presumed to maintain itself as a plane perpendicular to the flow. The payload is idealized as a point mass m_p with the entire volume of the vehicle devoted to heat-protection material. The heat-protection material is assumed to have a constant heat of sublimation ΔW.

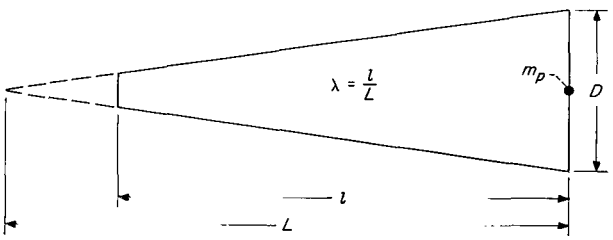

FIGURE 2.—Sketch of truncated cone.

Ballistic function $f(\lambda)$.—For the flat-faced cone in Newtonian flow the quantity C_DA is found to be

$$C_DA=\frac{\pi}{2}D^2\frac{(1-\lambda)^2+\left(\frac{D}{2L}\right)^2}{1+\left(\frac{D}{2L}\right)^2} \tag{4a}$$

The weight of the probe is found to be

$$ma_g=wV+m_pa_g=\frac{\pi}{3}wL^3\left(\frac{D}{2L}\right)^2[1-(1-\lambda)^3]+m_pa_g \tag{4b}$$

where V is the probe volume, w is the weight density, and m_p is the payload mass. The function $f(\lambda)$ thus becomes

$$f(\lambda)=\frac{a_gh_s'}{2\delta}=3\frac{a_gh_s'}{wL}\frac{1}{\frac{1}{1-\mu}-\frac{\mu}{1-\mu}(1-\lambda_{\infty-})^3-(1-\lambda)^3}\frac{(1-\lambda)^2+\left(\frac{D}{2L}\right)^2}{1+\left(\frac{D}{2L}\right)^2} \tag{4c}$$

so that

$$z=\frac{a_gh_s'}{wL} \tag{4d}$$

where $\mu=\frac{m_p}{m_{\infty-}}$ is the payload fraction and $\lambda_{\infty-}$ is the initial nondimensional size.

Heating function $g(\lambda)$.—The stagnation-point heating rates on a blunt body have the variations

$$q_{st,c}=\alpha\rho^mU^n\frac{1}{\sqrt{x}} \qquad \text{(Convective)} \tag{5a}$$

$$q_{st,r}=\beta\rho^rU^sx \qquad \text{(Radiative)} \tag{5b}$$

where x is a characteristic length of the body. (See, for example, refs. 4 and 5.) The values of the exponents indicated by references 4 and 5 are

$$\left.\begin{aligned} m&=\tfrac{1}{2}\\ n&=3\end{aligned}\right\}\text{Convective} \qquad \left.\begin{aligned} r&=2\\ s&=14\end{aligned}\right\}\text{Radiative} \tag{5c}$$

If heat inputs of the types indicated in relations (5a) and (5b) are considered to be operative, the rate of change of the nondimensional length λ is given by

$$-\frac{dV}{d\lambda}\dot{\lambda}=\frac{1}{w\Delta W}\int(q_r+q_c)dS=\frac{1}{w\Delta W}\left[\left(\frac{\bar{q}}{q_{st}}\right)_c q_{st,c}+\left(\frac{\bar{q}}{q_{st}}\right)_r q_{st,r}\right]S_{face} \tag{5d}$$

Equation (5d) assumes that all the heat input is effective in the sublimation process. In other words, conduction is neglected. When the relations (5a) and (5b) are introduced into (5d), the result is

$$-\frac{d\lambda}{d\rho}=\frac{h_s'}{w\Delta W}\left[\left(\frac{\bar{q}}{q_{st}}\right)_c\frac{\alpha}{L^{3/2}\sqrt{\frac{D}{L}}}\rho^{m-1}U^{n-1}\frac{1}{\sqrt{1-\lambda}}+\left(\frac{\bar{q}}{q_{st}}\right)_r\beta\frac{D}{L}\rho^{r-1}U^{s-1}(1-\lambda)\right] \tag{5e}$$

where the characteristic length x is the face diameter.

The rapid rise of the radiative term with velocity implies that for sufficiently high speeds the integrated heat input of the radiative term will dominate the input from the convective component. For sufficiently low speeds the contribution of the convective term will dominate. The case to be considered is that in which the contribution of the radiative term is dominant. Suppression of the convective term of equation (5e) yields the result

$$-\frac{d\lambda}{d\rho}=K\rho^{r-1}U^{s-1}(1-\lambda) \tag{5f}$$

where

$$K=\frac{h_s'}{w\Delta W}\left(\frac{\bar{q}}{q_{st}}\right)_r \beta\frac{D}{L} \tag{5g}$$

so that equation (3a) becomes

$$\frac{d^2\lambda}{d\omega^2}+[(s-1)e^{\omega}f(\lambda)-r]\frac{d\lambda}{d\omega}+\frac{1}{1-\lambda}\left(\frac{d\lambda}{d\omega}\right)^2=0 \tag{5h}$$

Numerical integrations of equation (5h) using the results of reference 5 ($r=2$, $s=14$) have shown that with steep entry and high mass loss, for practical probe sizes, the radiative heat inputs indicated by the radiative term of equation (5e) exceed the kinetic energy available in the flow except at the beginning and at the end of the trajectory. For completeness, however, the trajectory properties corresponding to equation (5h) are indicated in the appendix.

A physically acceptable radiative heat flux cannot exceed the flux of kinetic energy onto the face of the probe. This flux is

$$\frac{1}{2}\rho U^3$$

per unit area. Let the limiting radiative heat flux be written as

$$\frac{dQ}{dt}=\eta\frac{\rho}{2}U^3A_q \tag{5i}$$

An upper bound to the radiant heat flux is found if it is assumed, in coordinates moving with the probe, that all the incident energy flux is converted into photons, half of which enter the body and half of which escape. These assumptions require that

$$\eta\leq\frac{1}{2} \tag{5j}$$

and therefore the radiative heat input cannot exceed half the kinetic-energy flux. Because of the small range of validity of equation (5b) for the high-mass-loss trajectories to be considered, the heat-input function (5i) will be adopted. On comparing formula (5i) with (2b) the basic equation (3a) is seen to take the simple form

$$\frac{d^2\lambda}{d\rho^2}+2f(\lambda)\frac{d\lambda}{d\rho}=0 \tag{5k}$$

with

$$-\frac{d\lambda}{d\rho}=K'U^2 \tag{5l}$$

where

$$K'=\frac{h_s'}{w\Delta W}\frac{\eta}{2L} \tag{5m}$$

or, alternatively,

$$\frac{d^2\lambda}{d\omega^2}+[2e^{\omega}f(\lambda)-1]\frac{d\lambda}{d\omega}=0 \tag{5n}$$

with

$$-\frac{d\lambda}{d\omega}=K'e^{\omega}U^2 \tag{5o}$$

Limiting velocity.—For the separable equation (5k) a first integral may be obtained by quadrature as

$$\frac{d\lambda}{d\rho}+2\int f(\lambda)d\lambda=\text{Constant} \tag{6a}$$

and a second integral by quadrature as

$$\rho+(\text{Constant})'=\int\frac{d\lambda}{(\text{Constant})-2\int f(\lambda)d\lambda} \tag{6b}$$

If by definition

$$F(\lambda)=2\int_0^{\lambda}f(\lambda)d\lambda \tag{6c}$$

the first integration constant is found in terms of entry conditions as

$$\text{Constant}=F(\lambda_{\infty-})-K'U_{\infty-}^2 \tag{6d}$$

The limiting velocity is found directly as the value of $U_{\infty-}$ corresponding to $\frac{d\lambda}{d\rho}=0$ at $\lambda=0$:

$$U_l^2=\frac{F(\lambda_{\infty-})}{K'} \tag{6e}$$

On a ρ-z shift it is found that the limiting velocity

is independent of size L, weight density w, and effective scale height h_s'. In fact, the only indicated dependence is the following:

$$\frac{\partial \log U_l}{\partial \log \frac{\Delta W}{\eta}} = \frac{1}{2} \tag{6f}$$

Dynamic variables.—It is convenient to express the deceleration G and velocity U in terms of the solutions $\lambda(\rho)$. For the velocity we find

$$U^2 = -\frac{d\lambda}{d\rho}\Big/ K' \tag{7a}$$

and for the dimensionless acceleration

$$G = -\frac{\dot{U}}{a_g} = \frac{\rho f(\lambda)}{a_g h_s'} U^2 \tag{7b}$$

The peak acceleration occurs on the condition

$$\dot{G} = \frac{dG}{d\rho}\dot{\rho} = 0 \tag{7c}$$

Differentiating the right member of equation (7b) with respect to ρ and setting the derivative equal to zero gives, at the peak G condition,

$$2\rho f(\lambda) = 1 + \frac{d \log_e f(\lambda)}{d\lambda}\frac{d\lambda}{d\omega} \geqq 1 \tag{7d}$$

Relation (7d) is a generalization of that of the analysis of reference 6 wherein $2\rho f(\lambda)$ was found to be 1 at peak G for the case of constant shape and size.

Truncated cones.—Only the case of limiting velocity will be considered; therefore the integration constant of equation (6a) is zero when $F(\lambda)$ is used for the integral on the left-hand side. A closed form of the function $F(\lambda)$ can be obtained for truncated cones in terms of elementary functions, but the integral of equation (6b) leads to transcendental functions. The first integral is

$$F(\lambda) = 2\frac{a_g h_s'}{wLb^{2/3}}(1+a)^{-1}\left[-b^{2/3}\log_e(b-u^3) - a\log_e\frac{b^{1/3}-u}{\sqrt{b^{2/3}+b^{1/3}u+u^2}} + \sqrt{3}a\tan^{-1}\frac{\sqrt{3}u}{2b^{1/3}+u}\right]_{1-\lambda}^{1} \tag{8a}$$

where

$$a = \left(\frac{D}{2L}\right)^2 \geqq 0 \tag{8b}$$

$$b = \frac{1}{1-\mu}[1-\mu(1-\lambda_{\infty-})^3] \geqq 1 \tag{8c}$$

and for limiting velocity

$$U_l^2 = 4a_g\frac{\Delta W}{\eta}\frac{(1+a)^{-1}}{b^{2/3}}\left[-b^{2/3}\log_e(b-u^3) - a\log_e\frac{b^{1/3}-u}{\sqrt{b^{2/3}+b^{1/3}u+u^2}} + \sqrt{3}a\tan^{-1}\frac{\sqrt{3}u}{2b^{1/3}+u}\right]_{1-\lambda_{\infty-}}^{1} \tag{8d}$$

To maximize U_l^2 the value of $F(\lambda)$ must be as large as possible, which suggests that the integration of $f(\lambda)$ over λ, to which $F(\lambda)$ is proportional, should extend over as large a range as possible. However, the effect of the indicated extension of the range of integration is offset by a decrease in the value of the integrand at every λ. Calculations have shown that the effect of moving the integration limit is the larger. Therefore $\lambda_{\infty-}$ should be unity and the lower limit of the bracket in relation (8d) should be zero. Initially pointed cones are thus indicated as having the highest limiting velocities. As $a \to 0$, the limiting velocity indicated by relation (8d) approaches the value which, as shown in the next section, corresponds to a cylinder. At the other extreme ($a \to \infty$), corresponding to a shallow cone of zero length, the limiting velocity approaches the form

$$U_l^2 = 4a_g\frac{\Delta W}{\eta}\frac{1}{b^{2/3}}\left(\sqrt{3}\tan^{-1}\frac{\sqrt{3}}{1+2b^{1/3}} - \log_e\frac{b^{1/3}-1}{\sqrt{b^{2/3}+b^{1/3}+1}}\right) \tag{8e}$$

This result must be given a cautious physical interpretation. On the present model the drag

of the flanks is, in a sense, free, since no loss of material from the flanks is allowed. The relation (8e), corresponding to the limiting shallow cone, puts the highest possible drag in the place where it costs nothing. This consideration also applies, in a weaker form, to the earlier result which indicated that the pointed cone yields the highest limiting velocity. Only for flank slopes so shallow that the flank heat input is truly small compared with the face input can the present model be considered valid. The infinitely shallow cone obviously does not meet this requirement. A quantitative estimate of the flank input is given in the appendix.

For the second integral (eq. (6b)), with $\rho=0$ at $\lambda=\lambda_{\infty-}$,

$$\rho=\int_{\lambda}^{\lambda_{\infty-}}\frac{d\lambda}{F(\lambda)} \tag{8f}$$

Cylinders.—The case of a cylinder corresponds to that of a truncated cone for which $D/L\to 0$ and $L\to\infty$. If L is redefined as the original cylinder length ($\lambda_{\infty-}$ is thus always unity),

$$C_DA=\frac{\pi}{2}D^2 \tag{9a}$$

$$V=\frac{\pi}{4}D^2L\lambda \tag{9b}$$

$$f(\lambda)=\frac{a_gh_s'}{wL}\left(\lambda+\frac{\mu}{1-\mu}\right)^{-1} \tag{9c}$$

$$z=\frac{a_gh_s'}{wL} \tag{9d}$$

The function $F(\lambda)$ is

$$F(\lambda)=\frac{2a_gh_s'}{wL}\log_e\left(1+\frac{1-\mu}{\mu}\lambda\right) \tag{9e}$$

and the limiting velocity is given by

$$U_l^2=4a_g\frac{\Delta W}{\eta}\log_e\frac{1}{\mu} \tag{9f}$$

The absence of D/L (now the diameter-length ratio) indicates that there are no preferred proportions. Thus wafers and rods have the same limiting velocities. (Since C_DA has a large value at every value of λ, the cylinder yields high limiting velocities.)

Sphere.—The case of the homogeneous shrinking sphere was treated in reference 7. If this spherical configuration is formally converted into a space probe by addition of a point mass at the center of the sphere the function $f(\lambda)$ becomes

$$f(\lambda)=\frac{3}{8}\frac{a_gh_s'}{wR}\frac{\lambda^2}{\lambda^3+\frac{\mu}{1-\mu}} \tag{10a}$$

$$z=\frac{a_gh_s'}{wR} \tag{10b}$$

where $\lambda=r/R$ and $R=r_{\infty-}$. An integration yields

$$F(\lambda)=\frac{a_gh_s'}{4wR}\log_e\left(1+\frac{1-\mu}{\mu}\lambda^3\right) \tag{10c}$$

and the limiting velocity is

$$U_l^2=2a_g\frac{\Delta W}{\eta}\log_e\left(\frac{1}{\mu}\right) \tag{10d}$$

The limiting velocity for the modified solution of reference 7 is thus $\sqrt{2^{-1}}$ or 0.707 times the limiting velocity for the flat-faced cylinders. Again, as in the case of the cones and cylinders, there is no size dependency.

NUMERICAL RESULTS

For the cones the value $D/L=0.3$ has been adopted in the calculations. This value yields a shape that is slender enough to have little convection to the flanks (see appendix). The value $h_s'=25{,}200$ feet, which corresponds to vertical entry into the atmosphere, has been used throughout. The formulas of the analysis indicate the variation with h_s' of properties of interest. For example, the air loading G at each value of λ varies inversely with h_s'.

The limiting velocities indicated by the analysis for the limiting heat function are indicated in figure 3. Certain cases may be cited as examples. With a cylinder made of a material such as graphite ($\Delta W\approx 15{,}000$ Btu/lb), a payload fraction μ of $e^{-1}=0.368$, and $\eta=1/2$, the indicated limiting velocity is about 55,000 feet per second (fig. 3(c)), which is about the launch speed for escape from the solar system. For the η value of 1/4, the limiting value jumps to 78,000 feet per second, some 40 percent higher than launch speed for solar-system escape, and well beyond the 50,000- to 60,000-feet-per-second range suggested in reference 2. The results of reference 8 indicate smaller mean values of η than 1/4 for the high densities and speeds experienced in the region of high mass loss.

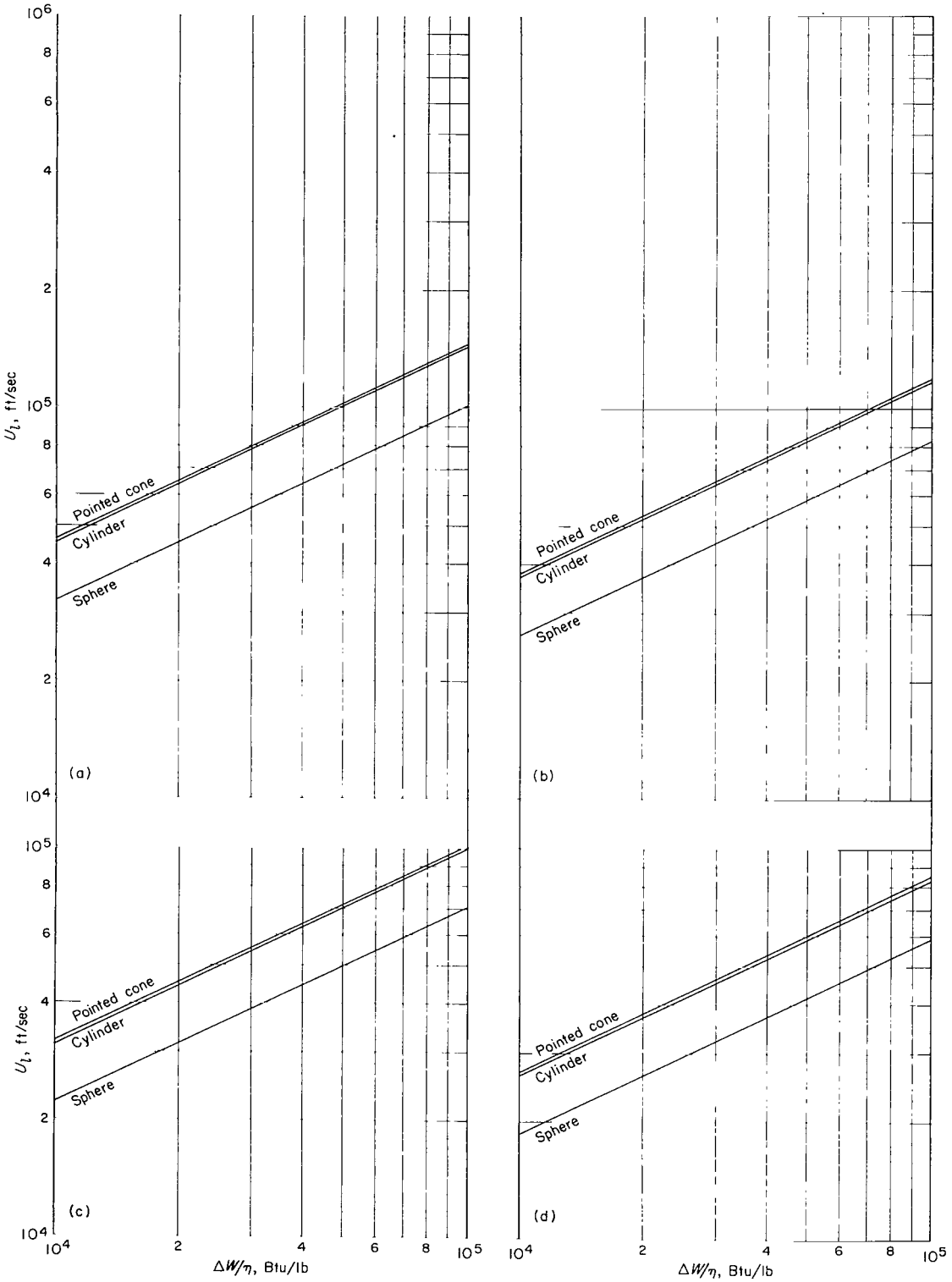

(a) $\mu = 1/8$.
(b) $\mu = 1/4$.
(c) $\mu = e^{-1}$.
(d) $\mu = 1/2$.

FIGURE 3.—Limiting velocity for various probes.

The unbounded increase of limiting velocity with vanishing payload implies that there is, in principle, no limit to the payload size or entry speeds possible. The payload fraction need only be decreased to that corresponding to the desired entry velocity and a large enough probe constructed to realize the assumed fractional value. Aside from the fact that there are practical limits on the size of probe which may be launched, there is, more fundamentally, the limited thickness of the earth's atmosphere to be considered.

With increasing probe size the position of the high-mass-loss region moves to lower altitudes. It should be recalled, however, that the air loads and limiting velocity do not change with size (eqs. (6e) and (6f)). A convenient reference point near the end of the high-mass-loss region is the peak G point. For some size of probe the peak G point will occur at sea-level density ($\omega=-6.03$ in English units). For sizes larger than those which put the peak G point at sea level, survival is clearly impossible. In figure 4 the size limitation imposed by the finite depth of the atmosphere is indicated in terms of the location of the peak G point as a function of size and payload fraction with $w=140$ lb/cu ft. For weight densities other than 140 lb/cu ft, figure 4 applies if the actual value of L is multiplied by $w/140$. The characteristic length used for the shrinking sphere is the diameter $2R$.

If the evidence of figure 4 is regarded as sufficient, it might be said that at $\mu=1/2$ a limiting size of $L\approx 20$ feet exists for the pointed cone and the cylinder, and a somewhat smaller value for the shrinking sphere (fig. 4(d)). However, the width of the high-mass-loss region must be considered. This width varies with probe shape so that a separate limiting size is indicated for each probe shape. The discussion will be limited to the case of $\mu=1/2$, which is the least favorable of the cases presented in the sense that higher payload fractions lead to smaller limiting probe sizes.

The width of the high-mass-loss region is indicated in figure 5 in terms of the G pulse experienced by the various probes. The shape of the G pulse has a characteristic form independent of the size L and the probe material as represented by w and ΔW, but dependent on the probe shape represented by $f(\lambda)$. The pulse shapes are seen to vary from narrow, in the case of the pointed cone, to extremely broad, for the case of the sphere. The difference in pulse width is associated with the differing behavior of $f(\lambda)\propto\delta^{-1}$ as the size λ goes to zero. For the pointed cone, the value of the ballistic parameter δ approaches a finite limit, while for the sphere, δ becomes infinite with vanishing radius.

Since all the pulses are actually of infinite breadth, the position of the peak G point does not actually mark the end of the high-mass-loss regions. Figure 5(d) indicates the deceleration to be essentially complete within about a scale height of the peak G point for the pointed cone and within about two scale heights for the cylinder. The decay of the G pulse is so much slower for the case of the shrinking sphere that no values of decay length or limiting size will be given for the sphere. Use of the decay lengths for the cone and cylinder in conjunction with figure 4(d) indicates a limit of $L\approx 7$ feet for the pointed cone and $L\approx 2.5$ feet for the cylinder. The corresponding probe weights for $w=140$ lb/cu ft and $D/L=0.3$ are 2×10^3 pounds for the pointed cone and 3×10^2 pounds for the cylinder. Increase of the diameter does not affect the position of the high-mass-loss region in the case of the cylinder.

The no-loss curve of figure 5 is taken from reference 5. It may be noted that low-mass-loss entry leads to a G pulse that is broad compared with that experienced in the high-mass-loss entry of cylinders and pointed cones. Only the high-mass-loss sphere has a broader G pulse.

The increase of pulse breadth with increasing μ indicated by figure 5 is associated with the increase of inertia of the payload with μ. In analytical terms, the value of $f(\lambda)$ is lowered at every λ value by increase of μ.

The values of peak G are indicated in figure 6 for a range of values of $\Delta W/\eta$, the effective heat capacity. The peak G value (and all other G values at a given value of λ) is proportional to the quantity $\Delta W/\eta$. Limiting velocity is thus unbounded for unlimited increase in effective heat capacity as well as for vanishing μ. However, the position of the high-mass-loss region does not shift with $\Delta W/\eta$, but rather with size L, as already shown in figure 4. Although the pointed cone with $D/L=0.3$ has only a slightly higher limiting velocity than the cylinder, it is subject to considerably higher loadings. These higher loadings are associated with the absence of high C_DA values until late in the trajectory for the case of the pointed cone.

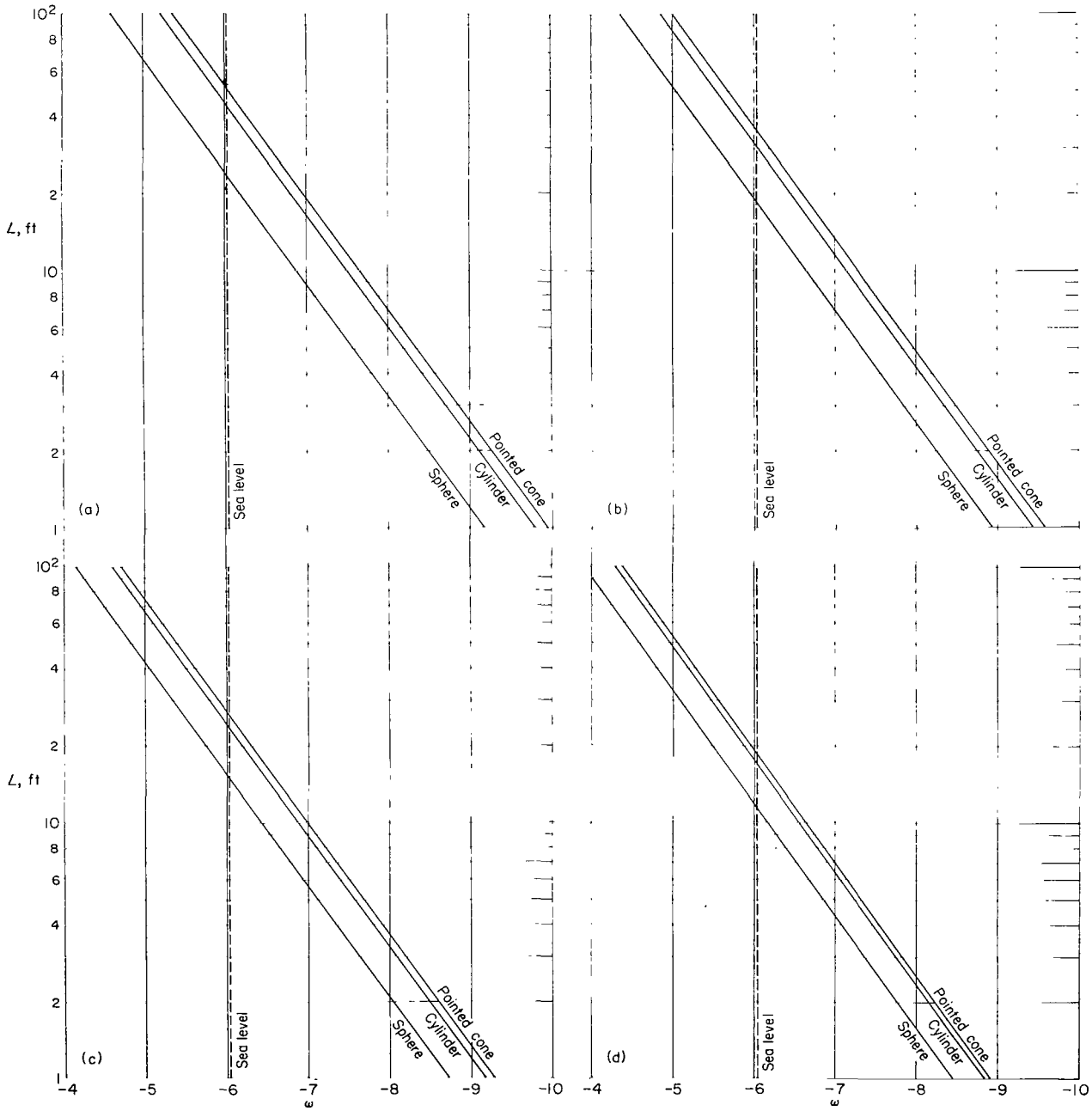

(a) $\mu=\frac{1}{8}$.

(b) $\mu=\frac{1}{4}$.

(c) $\mu=e^{-1}$.

(d) $\mu=\frac{1}{2}$.

FIGURE 4.—Location of peak G point for various probes. $w=140$ lb/cu ft.

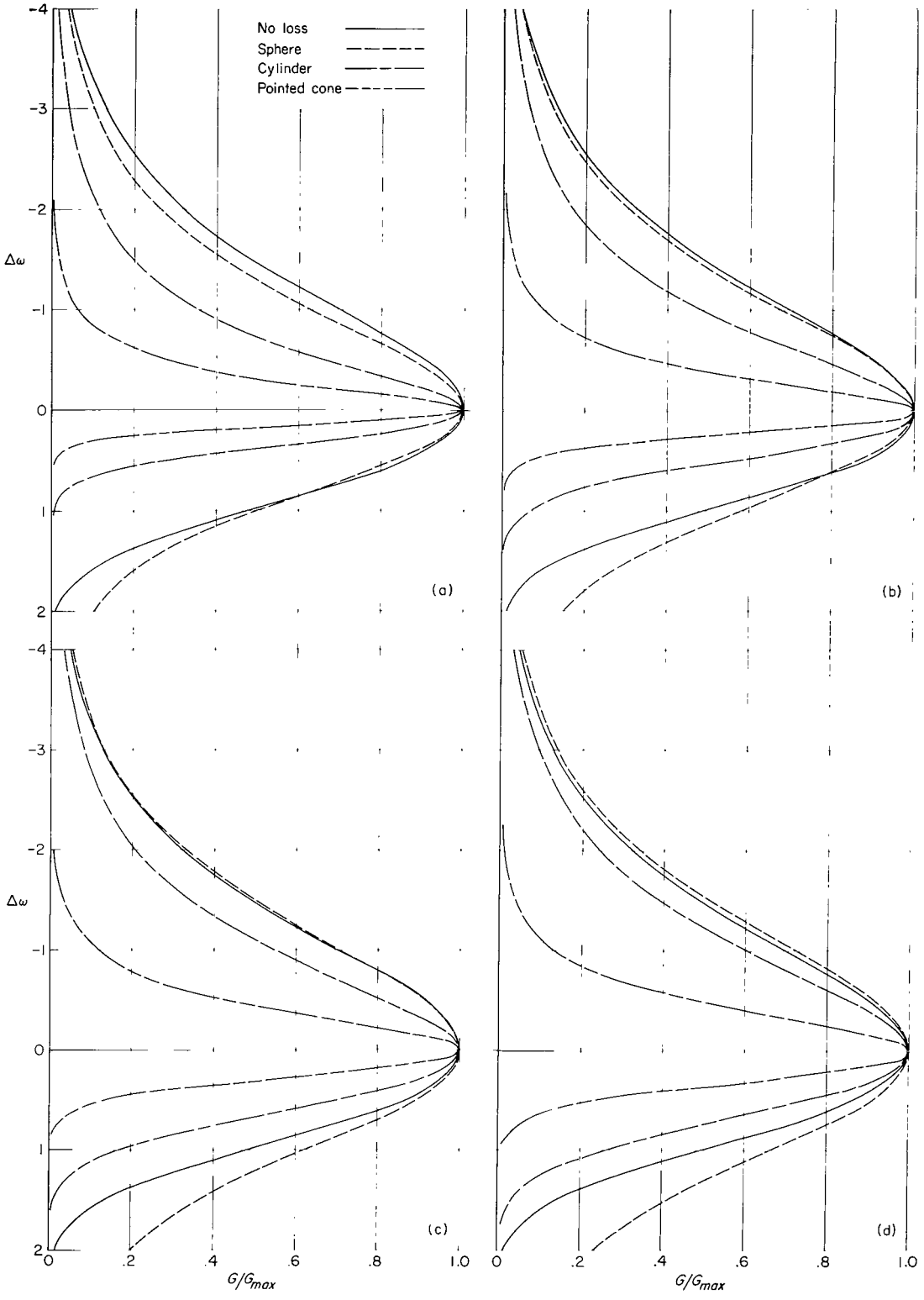

(a) $\mu=\frac{1}{8}$. (b) $\mu=\frac{1}{4}$.
(c) $\mu=e^{-1}$. (d) $\mu=\frac{1}{2}$.

FIGURE 5.—Shape of G pulse for various probes.

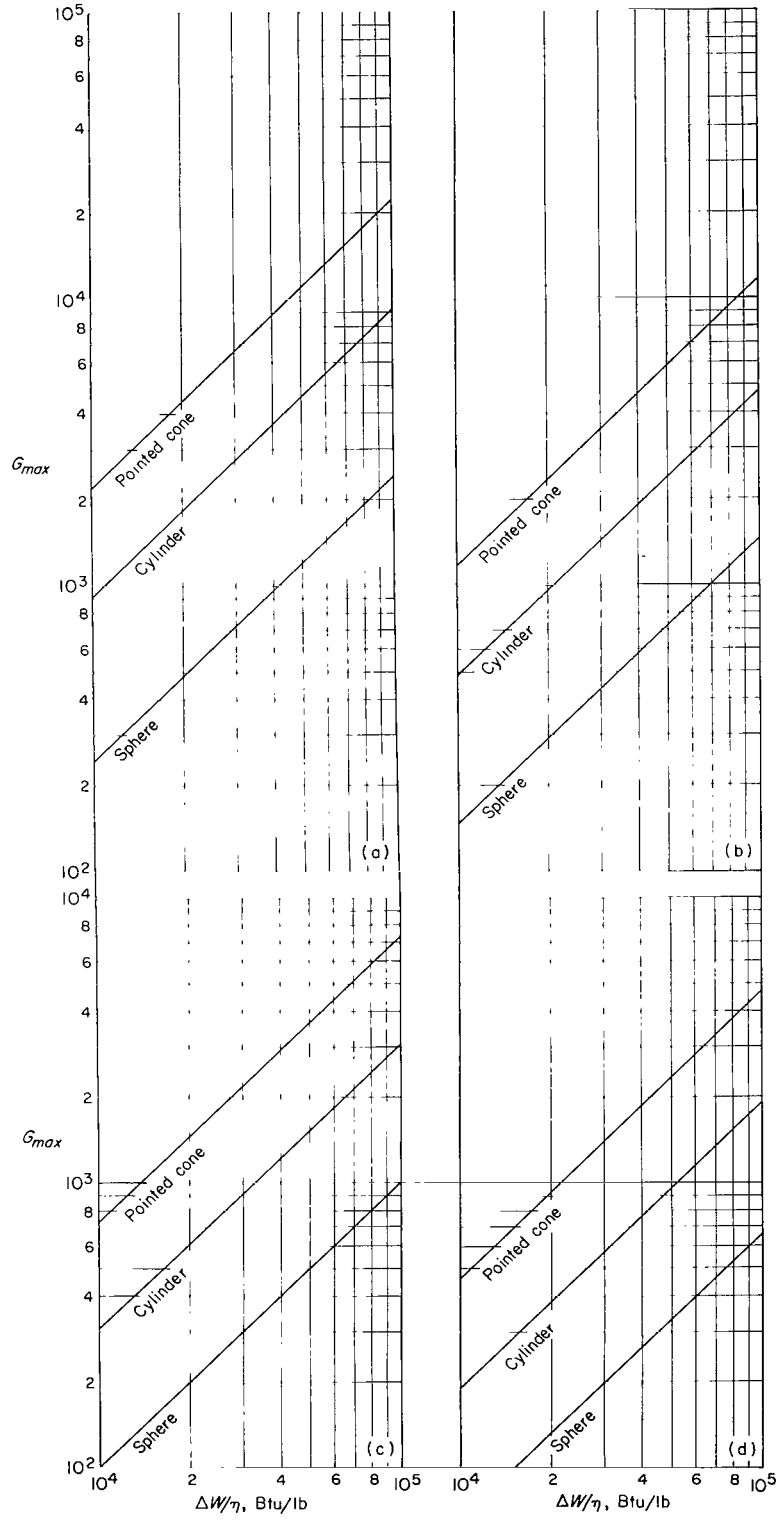

(a) $\mu=\frac{1}{8}$. (b) $\mu=\frac{1}{4}$.
(c) $\mu=e^{-1}$. (d) $\mu=\frac{1}{2}$.

FIGURE 6.—Value of peak G for various probes.

Although the limiting velocity of the pointed cone tends to increase with cone angle, the limiting velocity is bounded, in the present analysis, even for the case of the infinitely shallow cone. The values of the limiting velocity of the pointed cone, in units of the limiting velocity of a cylinder, are indicated in the following table for several values of μ.

μ	Ratio of limiting velocities of pointed cone and cylinder for D/L of—					
	0	0.3	0.6	1.2	2.4	∞
$\frac{1}{8}$	1	1.011	1.042	1.124	1.259	1.412
$\frac{1}{4}$	1	1.013	1.051	1.152	1.316	1.497
e^{-1}	1	1.015	1.058	1.170	1.352	1.550
$\frac{1}{2}$	1	1.017	1.062	1.188	1.384	1.598

When $\mu<\frac{1}{2}$ the limiting velocity of the zero-length cone ($D/L=\infty$) is less than 60 percent greater than that of the cylinder. The slender pointed cone with $D/L=0.3$ (cone half-angle of 8.5°) has a limiting velocity less than 2 percent higher than that of the cylinder when $\mu<\frac{1}{2}$. For other cones slender enough to permit neglect of the heat input to the flanks, similar small gains are indicated.

DISCUSSION OF ANALYSIS

The case of meteorlike bodies appears in the present analysis as the limiting case of vanishing payloads $\mu\to 0$. In this limit, for all three kinds of bodies considered (blunted cones, cylinders, and shrinking spheres) the limiting velocity becomes infinite. In fact, for all heat-input functions corresponding to $r\geqq 1$ and $s\geqq 3$, it can be shown that the limiting velocity becomes infinite as $\mu\to 0$. To obtain finite values of limiting velocity at $\mu=0$, a value of $\lambda_{\infty+}>0$ must be used as the defining value.

A convenient way of considering the heat inputs for atmospheric entry is in terms of the initial kinetic energy of the body. For entries at limiting velocity the heat capacity of the body $H_{\infty-}$ divided by the initial kinetic energy of the body $T_{\infty-}$ at limiting velocity indicates the fraction of the initial kinetic energy of the body returned to the body as heat under the most extreme conditions of survival. For flat-faced cylinders, which yielded values of limiting velocity that are high for the class of probes considered in the present analysis, the ratio is found to be

$$\frac{H_{\infty-}}{T_{\infty-}}=\frac{1}{2}\eta\frac{1-\mu}{\log_e\frac{1}{\mu}} \tag{11a}$$

Again, there is singular behavior for the case of $\mu=0$, which corresponds to meteorlike bodies. The ratio $H_{\infty-}/T_{\infty-}$ can be made arbitrarily small for small enough values of μ. The singular behavior of limiting velocity as the payload vanishes emphasizes the distinction between the cases of meteor and probe entry. Equation (11a) may be interpreted as indicating effective values of η or of $\Delta W/\eta$. The effective values of η are approximated by

$$\eta\approx 2\frac{H_{\infty-}}{T_{\infty-}}\log_e\frac{1}{\mu}\qquad(\mu\ll 1) \tag{11b}$$

in the case of high mass loss, and by

$$\eta\approx 2\frac{H_{\infty-}}{T_{\infty-}}\qquad(\mu\approx 1) \tag{11c}$$

for the case of low mass loss. Alternatively, effective values of $\Delta W/\eta$ are given by

$$\frac{\Delta W}{\eta}=\frac{1}{\log_e\frac{1}{\mu^2}}\frac{U_{\infty-}^2}{2a_0} \tag{11d}$$

which becomes, for low mass loss,

$$\frac{\Delta W}{\eta}\approx\frac{1}{2(1-\mu)}\frac{U_{\infty-}^2}{2a_0}\qquad(\mu\approx 1) \tag{11e}$$

According to the analysis there is no effect of size on limiting velocity, at least for the limiting form of the heat function. The only effect of increasing size is a lower altitude for the high-mass-loss region. On a limiting trajectory all the volume must be consumed, in the present model, and when more volume is provided a longer path is required for complete consumption when the initial velocity is the same in every case.

Although the anticipated advantage of the slender probe is borne out by the fact that pointed cones yield the highest limiting velocity, a physical interpretation must be made carefully. The neglect of heat input to the flanks causes the analysis to show an advantage for the largest flank area, which occurs on the pointed cone. Among pointed cones, those with the steepest flanks ($a \to \infty$), and consequently the highest flank drag, have highest limiting velocity. This result follows from the fact that $\frac{\partial f(\lambda)}{\partial a} \geqq 0$ in the interval $0 \leqq \lambda \leqq 1$. Obviously the flank input cannot be neglected on such shallow cones. For initially pointed cones which are so slender that the flank input is small compared with the face input, the limiting velocity is not much higher than that of flat-faced cylinders. It can be shown by integration of the proper $f(\lambda)$ that another shape with the same limiting velocity as a flat-faced cylinder is a pointed cone traveling base foremost.

Insofar as shape is concerned, the key requirement for high limiting velocity is a high value of the integral

$$\int_0^{\lambda_\infty} -\frac{d\lambda}{\delta} \tag{11f}$$

or, in other words, a high value of the mean reciprocal of the ballistic parameter with respect to the changing size of the vehicle. This may be more clearly seen, perhaps, if the ratio of equation (1g) to equation (5o) is taken, with the result

$$\frac{-\frac{dU}{d\omega}}{-\frac{d\lambda}{d\omega}} = \frac{\frac{a_g h_s'}{2\delta}\rho U}{\frac{h_s'}{w\Delta W}\frac{\eta}{2L}\rho U^2} \tag{11g}$$

or

$$d(U^2) = 2a_g \frac{\Delta W}{\eta}\frac{wL}{\delta} d\lambda \propto \frac{d\lambda}{\delta} \tag{11h}$$

which shows in a differential form the advantage of small δ.

CONCLUDING REMARKS

The analysis has shown that, for a limiting heat-input function and a simple probe model, there is no limit to the size of probe that may survive entry to the earth's atmosphere except that imposed by the finite depth of the atmosphere. In the absence of a payload there was found to be no limit to the possible entry speed. This zero-payload case corresponds to that of meteor entry. For finite payload fractions, entry speeds considerably in excess of the launch speed for solar-system escape were found to be possible.

The form of probe for highest entry speed was expected to be slender. This expectation was borne out when the analysis indicated that slender pointed cones have the highest value of limiting speed for the class of probes considered. However, the entry speed for cylinders was nearly as high and was independent of the cylinder proportions, so that wafers and rods have the same values. The indicated slight advantage of the slender cone was thought to come, in part at least, from the form of the analytical model and not from any real physical advantage. In sum, for the extreme case of high-mass-loss entries there is, in the present analysis, no clear indication of desirable proportions. The fact that high entry speeds were found for the cylindrical probes suggests that the blunt body indicated for low-mass-loss entries in which convective heat transfer is dominant may again be suitable in the extreme case of high-mass-loss entries in which radiative heat transfer is dominant.

LANGLEY RESEARCH CENTER,
NATIONAL AERONAUTICS AND SPACE ADMINISTRATION,
LANGLEY STATION, HAMPTON, VA., *November 29, 1962.*

APPENDIX

FUNCTIONAL RELATIONS, SCALING LAWS, AND ESTIMATES OF FLANK HEAT INPUTS

As mentioned in the discussion of the heating function $g(\lambda)$, the experimental variation of radiative heating obtained from reference 4, which indicates values of $r=2$ and $s=14$, leads to excessive values of radiative heating at the densities and speeds of steep high-mass-loss entries for practical probe sizes. However, the analysis holds for other values of r and s as long as the stagnation-point heating rate is proportional to the size of the face. The trajectory properties corresponding to $g(\lambda)=K(1-\lambda)$ thus may have some future interest. Under a ρ-z shift the following functional relations are found by use of equations (3d) and (7b):

$$\left(\frac{w}{h_s'}\right)^{r-1}\left(\frac{L}{a_g}\right)^{r}U^{s-1}=\text{Constant} \tag{A1}$$

$$GL^{\frac{2r}{s-1}}w^{\frac{2(r-1)}{s-1}}a_g{}^{1-\frac{2r}{s-1}}(h_s')^{1-\frac{2(r-1)}{s-1}}=\text{Constant} \tag{A2}$$

so that, specifically,

$$\frac{\partial \log U}{\partial \log L}=-\frac{r}{s-1} \tag{A3}$$

$$\frac{\partial \log G}{\partial \log L}=-\frac{2r}{s-1} \tag{A4}$$

For limiting velocities there is thus a size effect favoring smaller sizes (which might be expected since the heating per unit area is proportional to size) on the assumed heat-input function.

The formulas (A1) and (A2) derived for the function $g(\lambda)=K(1-\lambda)$ apply for the function $g(\lambda)=K'$ if in the exponent of L the quantity r is replaced by $r-1$. The corresponding functional relations on a ρ-z shift for the case of $g(\lambda)=K'$ may thus be written immediately as

$$\left(\frac{w}{h_s'}\right)^{r-1}a_g{}^{-r}L^{r-1}U^{s-1}=\text{Constant} \tag{A5}$$

$$G(wL)^{\frac{2(r-1)}{s-1}}a_g{}^{1-\frac{2r}{s-1}}(h_s')^{1-\frac{2(r-1)}{s-1}}=\text{Constant} \tag{A6}$$

and

$$\frac{\partial \log U}{\partial \log L}=-\frac{r-1}{s-1} \tag{A7}$$

$$\frac{\partial \log G}{\partial \log L}=-\frac{2(r-1)}{s-1} \tag{A8}$$

For the limiting heat function $g(\lambda)=K'$ the associated exponents are $r=1$ and $s=3$; therefore relations (A7) and (A8) indicate the absence of a size effect on limiting velocity. This is consistent with the fact that the assumed heat input per unit area for $g(\lambda)=K'$ is independent of size.

Independently of the assumed heat function, for the blunted cones and the cylinders, the position of the high-mass-loss region moves on a ρ-z shift according to the condition

$$\rho\frac{a_g h_s'}{wL}=\text{Constant} \tag{A9}$$

or

$$\frac{\partial \omega}{\partial \log_e \dfrac{wL}{a_g h_s'}}=1 \tag{A10}$$

The effect of an increase in size is to put the high-mass-loss region at lower altitudes. Changes in w, a_g, and h_s' are equivalent to size changes, the direction of the equivalent change being indicated by equation (A10).

In the direction of smaller sizes, the effect of convection will become relatively more important since the ratio of convective heating rate to radiative heating rate increases as $\rho^{-1/2}$ for the limiting form of the heat function and at a higher rate for the experimental variation of reference 4. If the convective input to the face is regarded as a perturbation and evaluated at every point of a trajectory established under radiation dominance, the limits of radiation dominance may be found. The convective heating rate to the face is

$$\dot{Q}_c=\frac{\pi}{4}\left(\frac{D}{L}\right)^{3/2}\left(\frac{\bar{q}}{q_{st}}\right)_c\alpha\rho^m U^n L^{3/2}(1-\lambda)^{3/2} \tag{A11}$$

The integrated convective input to the face of the blunted cones is thus

$$Q_c=\frac{\pi}{4}h_s'\left(\frac{\bar{q}}{q_{st}}\right)_c\alpha\left(\frac{D}{L}\right)^{3/2}L^{3/2}\int_{-\infty}^{\infty}\rho^m U^{n-1}(1-\lambda)^{3/2}d\omega \tag{A12}$$

The ratio of convective to radiative inputs for limiting trajectories is found to be

$$\frac{Q_c}{Q_r}=3\frac{h_s'}{w\Delta W}\left(\frac{\bar{q}}{q_{st}}\right)_c\alpha\left(\frac{D}{L}\right)^{-1/2}L^{-3/2}[1-(1-\lambda_{\infty-})^3]^{-1}\int_{-\infty}^{\infty}\rho^m U^{n-1}(1-\lambda)^{3/2}d\omega \tag{A13}$$

since, for limiting trajectories, Q_r is the heat capacity of the probe volume.

When the ratio Q_c/Q_r is evaluated for one limiting trajectory, it can be scaled to all other values of L by applying the ρz=Constant change which yields the following scaling laws for the case of $g(\lambda)=K(1-\lambda)$:

$$\frac{\partial \log Q_r}{\partial \log L}=3 \tag{A14}$$

$$\frac{\partial \log Q_c}{\partial \log L}=\frac{3}{2}+m-\frac{(n-1)r}{s-1} \tag{A15}$$

$$\frac{\partial \log \frac{Q_c}{Q_r}}{\partial \log L}=-\frac{3}{2}+m-\frac{(n-1)r}{s-1} \tag{A16}$$

and for the case of $g(\lambda)=K'$:

$$\frac{\partial \log Q_r}{\partial \log L}=3 \tag{A17}$$

$$\frac{\partial \log Q_c}{\partial \log L}=\frac{3}{2}+m-\frac{(n-1)(r-1)}{s-1} \tag{A18}$$

$$\frac{\partial \log \frac{Q_c}{Q_r}}{\partial \log L}=-\frac{3}{2}+m-\frac{(n-1)(r-1)}{s-1} \tag{A19}$$

For the calculations made with the limiting heat function $g(\lambda)=K'$, the associated exponents are $r=1$ and $s=3$ so that the last members of equations (A18) and (A19) vanish. By use of either equation (A16) or (A19) and the value of Q_c/Q_r for a single trajectory the value of L at which $Q_c\approx Q_r$ may be found. With a limiting trajectory for $g(\lambda)=K'$, a blunted cone of $L=8$ feet, and $\lambda_{\infty-}=0.70$, the ratio Q_c/Q_r is found to be 3×10^{-3}. After extrapolation to unit ratio by use of equation (A19) the corresponding value of L is 3×10^{-2} feet. This length is small enough to be out of the range of conceivable probe sizes and, in fact, beyond the scope of the analysis.

For the cylindrical shapes on the heating function $g(\lambda)=K(1-\lambda)$ there is an indicated choice of proportions which does not appear on the limiting function $g(\lambda)=K'$. If a given amount of heat-protection material is considered, a volume constraint of the form

$$D^2L=\text{Constant} \tag{A20}$$

is implied. If L is regarded as variable at constant volume, and it is recalled that $\frac{d\lambda}{d\omega}\propto\frac{D}{L}$ for $g(\lambda)=K(1-\lambda)$, a ρ-z change results in

$$L^{r-\frac{3}{2}}U_l^{s-1}=\text{Constant} \tag{A21}$$

When $r>3/2$, it is found that $U_l\to\infty$ for $L\to0$ and the cylinder becomes an infinitely thin wafer of infinite diameter. When $r<3/2$, $U_l\to\infty$ for $L\to\infty$ and the cylinder becomes an infinitely long needle of zero diameter. The high-mass-loss regions for the two cases are at $\omega=-\infty$ for the wafer and at $\omega=\infty$ for the rod. For the limiting function $g(\lambda)=K'$, the limiting velocity was shown to be independent of the proportions.

The relative heat inputs to the face and to the flanks of the truncated cones can be roughly estimated. If, in the case of convection, the flank input is considered to be the same at each axial station as that to a swept cylinder with the same radius as the local cone radius, and the loss of material on the flanks is neglected, it turns out that

$$\frac{(Q_c)_{flanks}}{(Q_c)_{face}}<1.6 \tag{A22}$$

so that the flank input can be greater than, but remains comparable to, the face input. The regime of radiation dominance on the face thus implies dominance on the vehicle.

Let the radiative input to the flanks be put on the same basis as that to the face. That is, let the fraction η of the kinetic energy of the impinging flow which is due to the component of free-stream velocity normal to the surface be converted into heat on the flanks. It is found, after integration, that

$$\frac{(Q_r)_{flanks}}{(Q_r)_{face}} < \frac{1}{2}\left(\frac{D}{L}\right)^2 \tag{A23}$$

For $D/L \leqq 0.3$ the flank input is less than 5 percent of the radiative face input according to relation (A23).

REFERENCES

1. Allen, H. Julian: Hypersonic Aerodynamic Problems of the Future. Presented to Fluid Mechanics Panel of AGARD (Brussels, Belgium), Apr. 3–6, 1962.
2. Öpik, Ernst J.: Physics of Meteor Flight in the Atmosphere. Interscience Publ., Inc. (New York), 1958.
3. Riddell, Frederick R., and Winkler, Howard B.: Meteorites and Re-Entry of Space Vehicles at Meteor Velocities. ARS Jour., vol. 32, no. 10, Oct. 1962, pp. 1523–1530.
4. Lees, Lester: Laminar Heat Transfer Over Blunt-Nosed Bodies at Hypersonic Flight Speeds. Jet Propulsion, vol. 26, no. 4, Apr. 1956, pp. 259–269, 274.
5. Thomas, P. D.: Air Emissivity and Shock-Layer Radiation. Jour. Aerospace Sci. (Readers' Forum), vol. 29, no. 4, Apr. 1962, pp. 477–478.
6. Allen, H. Julian, and Eggers, A. J., Jr.: A Study of the Motion and Aerodynamic Heating of Ballistic Missiles Entering the Earth's Atmosphere at High Supersonic Speeds. NACA Rep. 1381, 1958. (Supersedes NACA TN 4047.)
7. Hansen, C. Frederick: The Erosion of Meteors and High-Speed Vehicles in the Upper Atmosphere. NACA TN 3962, 1957.
8. Yoshikawa, Kenneth K., and Chapman, Dean R.: Radiative Heat Transfer and Absorption Behind a Hypersonic Normal Shock Wave. NASA TN D-1424, 1962.

U.S. GOVERNMENT PRINTING OFFICE:1964